Calculation of a Prismatic Body in the Form of a Spatial Beam under Various Boundary Conditions

Mukhammadaziz Rasulmukhammedov[1, 2], Shokhsanam Shukurova[1, 2] and Zamira Mirzayeva[1, 2]
[1]*Department of Information Systems and Technologies in Transport, Tashkent State Transport University, 100167 Tashkent, Uzbekistan*
[2]*University of Diyala, Baghdad Old Road, 32001 Diyala, Iraq*
prof.rasulmukhamedov@gmail.com, shoxsanamm2896@gmail.com, zmirzaeva83@mail.ru

Keywords: Spatial Prismatic Body, Elasticity, Flexibility Analysis, Finite Element Method (FEM), System of Algebraic Equations, Boundary Conditions.

Abstract: Because they are so strong and can hold a lot of weight, reinforced concrete beams are important parts of structures like foundations, walls, floors, and columns. Reinforced concrete structures include steel reinforcement bars that help the material resist both compressive and tensile forces. Because of this interaction, the steel and concrete form a strong structural system that is suitable for buildings designed to carry heavy loads. In applied mathematics, modeling the behavior of beam-like spatial bodies is a complex task because it requires solving systems of differential equations that describe deformation and stress in three-dimensional space. Modern computational mathematics, particularly numerical methods implemented with computer technologies, provides effective tools for solving such problems. In this study, prismatic finite-element meshes were developed to analyze static problems within the three-dimensional theory of elasticity. The proposed method was tested on several benchmark problems, and the results were compared with those obtained using the classical finite element method. The comparison confirmed that the method can accurately describe the mechanical behavior of spatial beam structures under different boundary conditions, making it useful for analyzing reinforced concrete elements.

1 INTRODUCTION

Reinforced concrete beams are widely used in construction due to their high strength, durability, and ability to carry significant loads. They are also resistant to fire, which increases the safety and reliability of buildings. The inclusion of steel reinforcement improves the performance of concrete by reducing bending and allowing the structure to withstand different types of mechanical stress.

Such beams are particularly suitable for buildings located in regions with high humidity or severe weather conditions. Reinforced concrete demonstrates good resistance to moisture, low temperatures, and other environmental influences. In addition, the combination of steel and concrete creates a stable structural system that can maintain its mechanical properties for a long period of time [1].

Because of these advantages, reinforced concrete beams are widely applied in large-scale construction projects, including bridges, tunnels, dams, and high-rise buildings. Their main purpose is to ensure the strength and long-term stability of structural elements.

The design of reinforced concrete beams may vary depending on the requirements of a particular project. They can be used in the form of beams, slabs, or columns, and their dimensions are usually determined by the expected loads and structural design parameters [2]. When selecting such elements, engineers typically consider factors such as mechanical strength, environmental resistance, ease of installation, and economic efficiency [3].

In computer-based structural analysis, meshing is an important step. Finite elements can be defined in one-, two-, or three-dimensional coordinate systems depending on the complexity of the model. Each element is characterized by nodes that determine its geometry and represent the degrees of freedom. In some cases, additional nodes are introduced to improve the accuracy of the approximation. Understanding these principles is essential when analyzing reinforced concrete beams using the finite element method [4].

2 MATERIALS AND METHODS

Automatic mesh generators facilitate effective modeling in modern finite element method modeling by utilizing a large number of linear elements with simple geometry as opposed to higher order elements which require manual definition. The geometry of each of the finite elements is defined based on the position of the nodes in the element. In this research work, the elements chosen are three-dimensional prisms with simple geometries. The unknown functions in the nodes or their derivatives with respect to spatial coordinates are considered the degrees of freedom [5], [6].

Defining boundary conditions is an important step in the finite element analysis process. When defining boundary conditions, displacements at nodes are fixed such that the finite element model behaves similar to the real structure being analyzed. Nodal displacements and loads are defined as boundary conditions only at the nodes. Special care is taken to define the minimum number of boundary conditions such that the performance of the structure is appropriately modeled [7].

The difficulties in solving the problem numerically with the use of finite element method arise because of complicated computations involved in the system of algebraic equations obtained. The amount of calculations depends both on the discretization of the computational domain and the selected basis functions. From these perspectives, one should note the benefits of six-faced finite elements over isoparametric parallelepiped elements, since they have similar accuracy properties but also allow for effective modeling of complicated boundaries [8].

For software meant to be used by experts in structural analysis, automatic computation throughout the entire computational process is a necessity, especially mesh generation. Automatic discretization is important not just because it removes the requirement for the expertise of the user in computational math but also because the efficiency of finite element computations depends heavily on its accuracy [9]. In many existing mesh generation softwares, a considerable amount of expertise is required from the user.

In some cases, the automatic generation of the hexagonal mesh can be realized through the direct division of the computational area into hexagonal meshes. When dealing with elasticity problems of the three-dimensional spatial body, the formation of the model in the form of a parallelepiped followed by the analysis of its deformation is applicable [10].

The final step involves carrying out computational tests and numerical modeling to define the stress-strain state of the spatial body in accordance with the defined boundary conditions. With the help of the FEM models, we can estimate deformation, internal forces, and stresses.

3 RESULTS

Beams and prismoidal bodies are quite popular structural objects used in construction and engineering works. This paper examines the stress and strain condition of a three-dimensional parallelepiped rigidly fixed by two opposite faces and loaded uniformly along its surfaces. Other faces had no external actions applied to them. The boundary conditions were as follows:

$$\begin{cases} u_1 = 0, u_2 = 0, u_3 = 0 & \text{if } x_3 = 0 \\ u_1 = 0, u_2 = 0, u_3 = 0 & \text{if } x_3 = c \\ \sigma_{11} = 0, \sigma_{12} = 0, \sigma_{13} = 0 & \text{if } x_1 = 0, a. \\ \sigma_{22} = 0, \sigma_{12} = 0, \sigma_{23} = q0 & \text{if } x_2 = b \\ \sigma_{22} = 0, \sigma_{12} = 0, \sigma_{23} = 0 & \text{if } x_2 = 0 \end{cases}$$

The geometry and material properties used for the first problem were: a=0.5 m (a - width); b=0.25 m; 0.5 m; 1.0 m (b - height); c=6.0 m; (c-length); E= $33*10^3$MPa (elastic modulus); μ=0.2 (Poisson's ratio); γ=0.5;1;2; (γ=b/a), β=0.69;0.83;0.16; (β =b/c), q_0 = -25 MPa. The finite element mesh consisted of 2000 elements and 2541 nodes, producing a system of 7623 linear algebraic equations with a bandwidth of 402. The discretization along the x, y, and z axes included 11, 11, and 21 divisions, respectively.

The displacement component U_2 at the midpoint of the beam (0.5a;0.5b; x_3) was analyzed for different heights b (Fig. 1, Table 1). Due to the cantilevered boundary condition, the displacement at the fixed surface was zero, while the maximum displacement at the loaded surface varied with the height b.

Table 1: Displacement component U_2 at the midpoint of the beam (0.5a,0.5b, x_3) for different heights b.

U_2 (0.5a;0.5b;0.5s)		
b=0.25m	b=0.5m	b=1.0m
-49.494166966	-1.5298175577	-1.5298175577

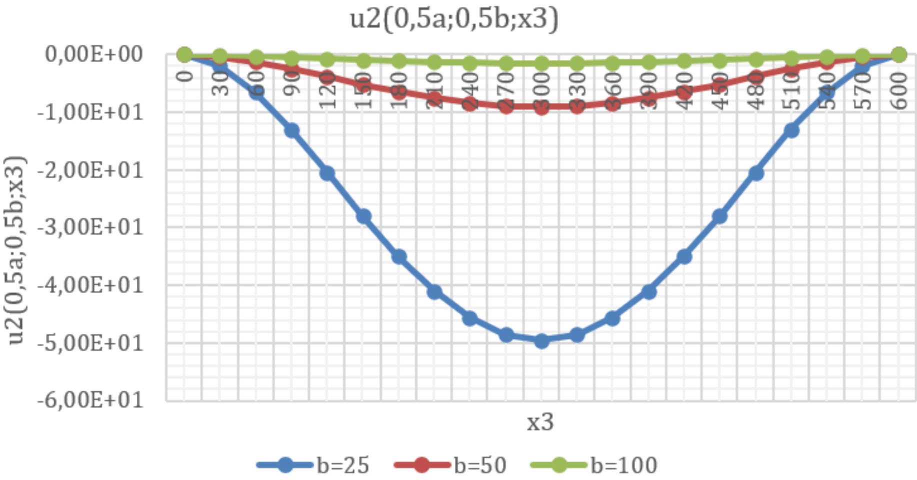

Figure 1: Displacement component U_2 at the midpoint of the beam $(0.5a,0.5b,x_3)$ for different heights b.

Table 2: Central axis displacements.

U_1 $(0.5a;0.5b;x_3)$					U_3 $(0.5a;0.5b;x_3)$			
x_3	β=0.69	V=0.83	V=0.16		x_3	β=0.69	V=0.83	V=0.16
0	0.00E+00	0.00E+00	0.00E+00		0	0.00E+00	0.00E+00	0.00E+00
30.	4.75E-13	-5.78E-14	9.66E-15		30.	-3.16E-04.	-5.19E-04.	-8.63E-04.
60.	1.44E-12	-1.95E-13	3.31E-14		60.	-1.57E-04	-2.63E-04.	-7.59E-04
90.	2.50E-12	-3.85E-13	6.69E-14		90.	-1.89E-04	-2.06E-04.	-4.59E-04
120.	3.67E-12	-6.30E-13	1.09E-13		120.	-1.51E-04	-1.92E-04	-3.03E-04
150.	4.51E-12	-8.73E-13	1.51E-13		150.	-1.26E-04.	-1.59E-04	-2.38E-04.
180.	4.54E-12	-1.10E-12	1.91E-13		180.	-1.01E-04	-1.27E-04.	-1.92E-04
210.	3.70E-12	-1.28E-12	2.21E-13		210.	-7.58E-05	-9.51E-05	-1.46E-04.
240.	1.10E-12	-1.44E-12.	2.47E-13		240.	-5.06E-05	-6.34E-05	-9.80E-05
270.	-2.16E-12	-1.57E-12	2.59E-13		270.	-2.53E-05	-3.17E-05	-4.91E-05
300.	-4.72E-12	-1.70E-12	2.59E-13		300.	2.41E-13	-6.32E-15	6.55E-16
330	-6.18E-12	-1.83E-12	2.47E-13		330	2.53E-05	3.17E-05	4.91E-05
360	-6.33E-12	-1.90E-12	2.23E-13		360	5.06E-05	6.34E-05	9.80E-05
390	-5.55E-12	-1.85E-12	1.92E-13		390	7.58E-05	9.51E-05	1.46E-04
4.20.	-4.51E-12	-1.63E-12	1.57E-13		4.20.	1.01E-04	1.27E-04	1.92E-04
450	-3.14E-12	-1.34E-12	1.24E-13		450	1.26E-04	1.59E-04	2.38E-04
480.	-2.30E-12	-9.71E-13	8.90E-14		480.	1.51E-04	1.92E-04	3.03E-04
5.10.	-1.37E-12	-6.21E-13.	5.61E-14		5.10	1.89E-04	2.06E-04	4.59E-04
540.	-6.71E-13	-3.13E-13	2.90E-14		540.	1.57E-04	2.63E-04	7.59E-04
570.	-1.99E-13	-9.45E-14	8.55E-15		570.	3.16E-04	5.19E-04	8.63E-04
600	0.00E+00	0.00E+00	0.00E+00		600	0.00E+00	0.00E+00	0.00E+00

On the central axis (x_1=0.5a, x_2=0.5b), the displacements U_1 and U_3 were approximately zero throughout the beam height. Detailed values of U_1 and U_3 at various heights x_3 and aspect ratios β are presented in Table 2.

Figure 2 shows the graph of the displacement U_3 (x_1,0.5b,x3) at x_3=0;0.3;0.6;.........6.0 m at x1=0;0.05;0.10;0.15;0.20;0.25 m. From the shown drawing, U_3 At the central axis points, i.e., (x_1=0.5a, x_2=0.5b, x_3), and in the prism regions where the fixed region has zero values in the x_3=0 and x_3=c planes, it has non-zero values, taking maximum values in the x_3=0.25c and x_3=0.75c planes.

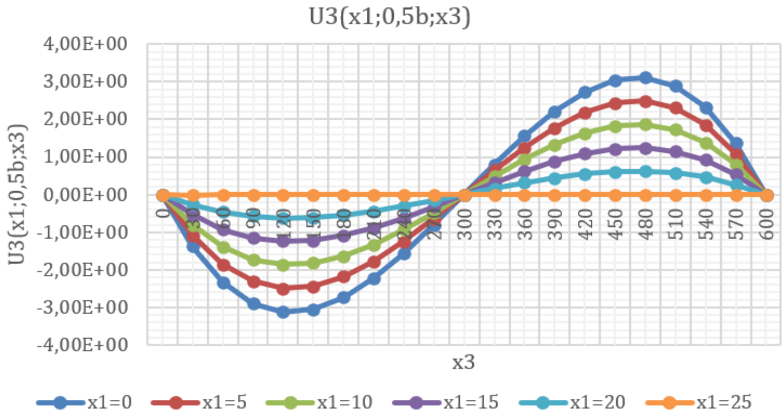

Figure 2: Displacement $U_3(x_1, 0.5b, x_3)$ along the beam for various heights x_3. Maximum deflection occurs near x_3=0.25c and x_3=0.75c, while zero displacement is observed at the fixed planes (x_3=0 and x_3=c).

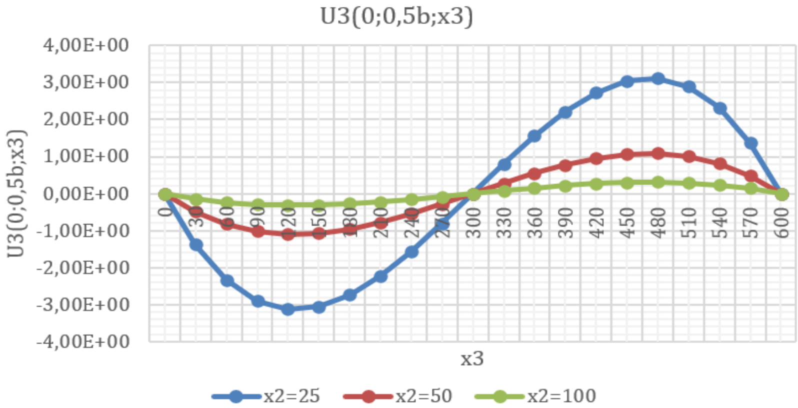

Figure 3: Displacement $U_3(0, 0.5b, x_3)$ along the side surface fordifferent aspect ratios γ=b/a. Displacement decreases along the side surface and reaches its maximum in the plane of applied load.

In Figure 3, U_3 (0; 0,5b; x_3) has different displacements γ=0.5; 1; 2; (γ=b/a), β=0.69; 0.83; 0.16; (β =b/c) is depicted in. On the side of the prismatic element, the values of the displacement decrease with height and reach a maximum value in the plane of application of the load.

In Figure 4, σ_{11} (0.5a; x_2; 0) values of the surface x_3=0 x_1=0.5a are shown in different γ=0.5; 1; 2; (γ=b/a), β=0.69; 0.83; 0.16; (β =b/c) is given in. It is possible to see the linear change of the central voltage, taking the value i. Similarly, the value of x_1=0.5a of the area x_3=c can be found in different γ=0.5; 1; 2; (γ=b/a), β=0.69; 0.83; 0.16; (β =b/c) is generated at.

In Figure 5 σ_{11} (0.5a; x_2; 0.5c) the voltage of the surface x_3=0.5c has different values x_1=0.5a γ=0.5; 1; 2; (γ=b/a), β=0.69; 0.83; 0.16; (β =b/c) is given in. It is possible to see the linear change of the central voltage, taking the value i.

In Figure 6, σ_{11} (0,5a; x_2; x_3) the voltage x_1=0,5a x_2=0; 0,b1; 0,2b; 0,3b; 0,4b; 0,5b and also x_3=0; 0,5c; x_3=0,10s;.....; x_3=1,00s; the value of is indicated by the length of the prism. It can be seen that the stress value σ_1 at the fixed surface is zero at the center and has a non-zero value as x_2 increases. However, x_3>=0.10s and x_3<=0.90s; is close to zero upward.

In Figure 7, the values of x_1=0; 0.02a; 0.04a; 0.05a; 0.06a; 0.08a; 0.10a and x_2=0; 0.1b; 0.2b; 0.3b; 0.4b. The graph of the displacement u_2 (x_1;x_2;0.5c) is presented for the values of 0.5b. From the shown graph, the displacement U_2 at x_3=0.5c for all values of x_1 and also at x_3=0.5c for all values of x_2 has parabolic values in the loaded region, i.e., takes a maximum value in the center.

In Figure 8, a=0.1m; b=0.4m; x_2=0; 0.1b; 0.2b; 0.3b; 0.4b; 0.58b; 0.6b; 0.7b; 0.86b; 0.9b; b and x_1=0; 0.1a; 0.2a; 0.3a; 0.4a; 0.5a; 0.6a; 0.7a; 0.8a. The graph of the displacement u_1 (x_1; x_2; c) for the values of 0.9a; a is presented. From the indicated drawing, taking the linear form U_1 in the direction of displacement x_1, we obtain √=0.5; Deviation from Kirchhoff's hypothesis at (β =b/c). In Figure 9, a=0.1m; b=0.4m; x_1=0; 0.02a; 0.04a; 0.05a; 0.06a; 0.08a; 0.10a and x_2=0; 0.1b; 0.2b; 0.3b; 0.4b; 0.5b; 0.6b; 0.7b; 0.8b. The graph of the displacement u_3 (x_1; x_2; c) for values of 0.9b; 1.0b is presented. From the shown graph, the displacement U_3 above x_2 =0.5b it takes a positive value, but at the lower value, it takes a negative value and changes linearly.

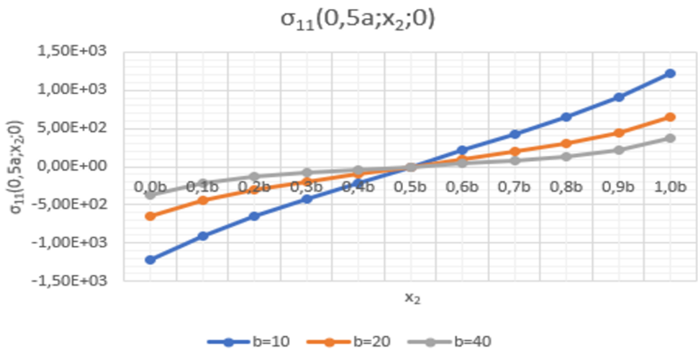

Figure 4: Stress distribution σ_{11}(0.5a, x_2, 0) on the surface x_3=0 for different aspect ratios γ and β. The central stress varies approximately linearly along x_2.

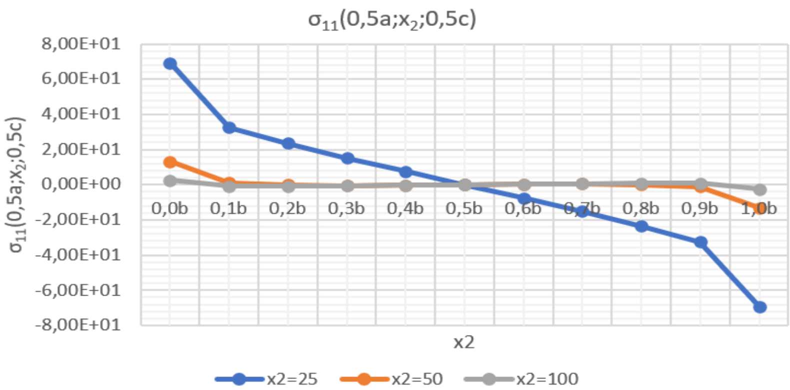

Figure 5: Stress distribution σ_{11}(0.5a, x_2, 0.5c) at mid-plane x_3=0.5c. Linear variation of stress along the central axis is observed, with higher stress near the loaded region.

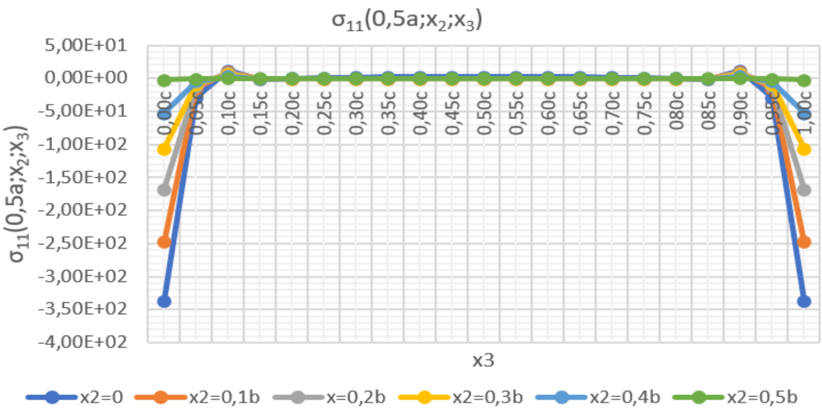

Figure 6: Three-dimensional stress distribution σ_{11}(0.5a, x_2, x_3) along the length and width of the beam. Stress is zero at the fixed surface center and increases towards the lateral faces, while near the top and bottom surfaces (x_3≤0.1c and x_3≥0.9c) the stress is negligible.

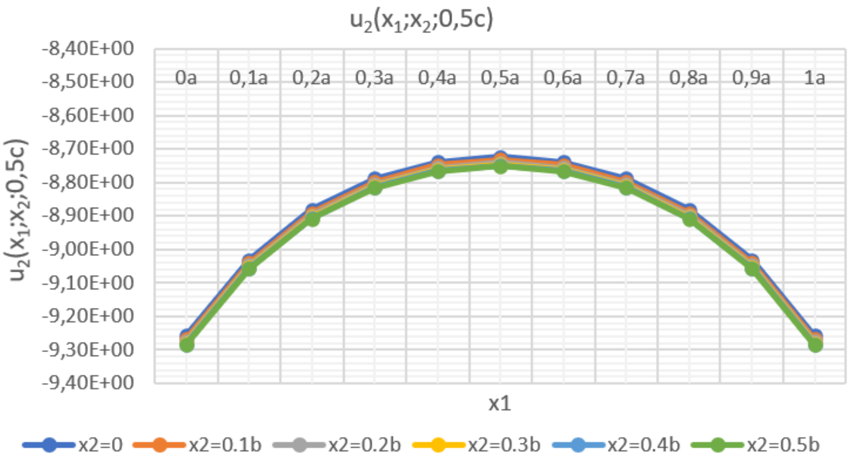

Figure 7: Transverse displacement $U_2(x_1,x_2,0.5c)$ showing a parabolic profile across the loaded region. Maximum deflection occurs at the beam center along both x_1 and x_2 directions.

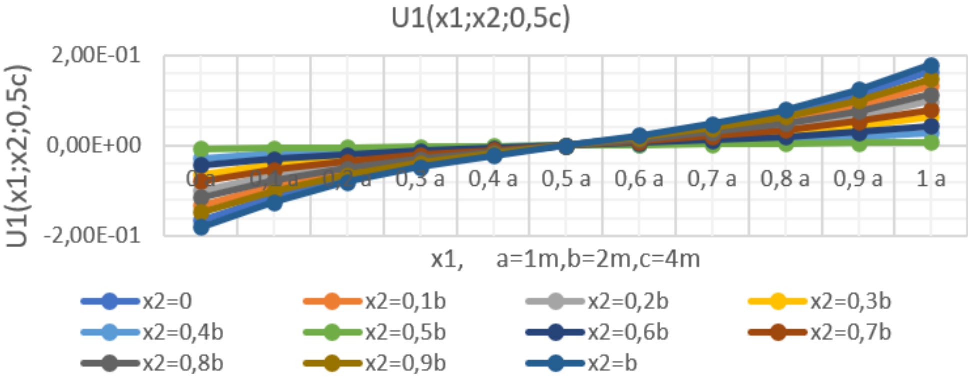

Figure 8: Longitudinal displacement $U_1(x_1, x_2, c)$ along the top surface of the beam. The displacement varies approximately linearly with minor deviations from Kirchhoff's hypothesis depending on the aspect ratio β.

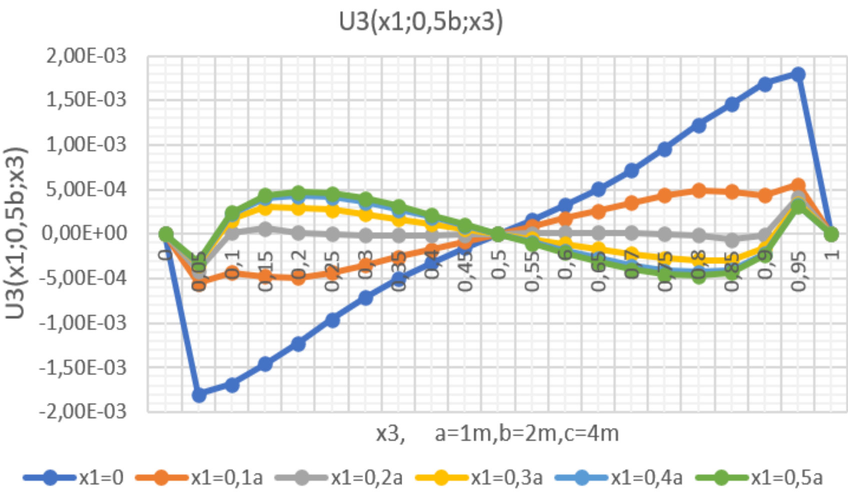

Figure 9: Longitudinal displacement U3(x1, x2, c) along the top surface of the beam. Displacement is positive above the central axis (x2=0.5b) and negative below, with approximately linear variation across the width.

4 CONCLUSIONS

A spatial beam is a body that is widely used in the construction industry, and it was considered how to simplify it in various boundary conditions, geometrically in different dimensions, when creating a computational model. In accordance with the set goal, existing methods for calculating reinforced concrete structures and test results were analyzed, taking into account the linear deformation of concrete, and a methodology for determining the stress-strain state of spatial reinforced concrete structures was developed.

The widespread popularity of the finite-element method and its transformation into one of the leading numerical methods for solving mechanical problems are associated with a number of advantages. The solved problems showed the following advantages of the finite-element method: the investigated prismatic objects can have different shapes and properties; finite elements were used in prismatic shapes; the linear properties of isotropic objects were investigated; stationary problems were solved; problems of various shapes and sizes were solved; boundary conditions of prismatic elements in the form of a console were modeled; the computational algorithm, presented in matrix form, was implemented uniformly regardless of various physical problems and the degree of dimensionality, and simplified computer programming for solving these problems; it facilitated the analysis of problems related to solving various physical problems on a single finite-element grid; hierarchical discretization of the investigated domain was carried out using superelements, which made it possible to effectively apply parallel computations in individual parts.

REFERENCES

[1] N. Fedorenko, B. N. Fedulov, and E. V. Lomakin, “Problem of loss of stability of thin-walled structures made of composite materials, the properties of which depend on the type of loading,” PNRPU Mechanics Bulletin, vol. 3, no. 12, pp. 104-111, 2019.

[2] R. D. Cook, D. S. Malkus, M. E. Plesha, and R. J. Witt, Concepts and Applications of Finite Element Analysis, 4th ed. New York, NY, USA: Wiley, 2002.

[3] V. I. Gorbachev and L. A. Kabanova, “Formulation of problems in the general Kirchhoff-Love theory of inhomogeneous anisotropic plates,” Moscow University Mechanical Bulletin, pp. 60-66, 2018.

[4] T. Hughes, The Finite Element Method: Linear Static and Dynamic Finite Element Analysis. Mineola, NY, USA: Dover Publications, 2000.

[5] M. M. Rasulmukhamedov, K. Sh. Tashmetov, and T. Sh. Tashmetov, “Modeling Traffic Flow Using the LWR Model and Finite Difference Numerical Method: Analysis of Efficiency and Applicability in Urban Transport Infrastructure Conditions,” in Sustainable Development of Transport: Economy, Transformation, Logistics and ESG Agenda, pp. 77-84, 2025.

[6] M. Rasulmuhammedov, S. Shukurova, and Z. Mirzayeva, “Analysis of the Elastic Stress-Strain Behavior of Complex-Shaped Three-Dimensional Bodies,” in Proceedings of the 13th International Conference on Applied Innovations in IT (ICAIIT), pp. 485-490, 2025.

[7] J. N. Reddy, Theory and Analysis of Elastic Plates and Shells. Boca Raton, FL, USA: CRC Press, 2007.

[8] A. A. Samarskiy, Introduction to Numerical Methods. Moscow, Russia: Lan’, 2009.

[9] S. P. Timoshenko and J. N. Goodier, Theory of Elasticity. New York, NY, USA: McGraw-Hill, 1970.

[10] O. C. Zienkiewicz, R. L. Taylor, and J. Z. Zhu, The Finite Element Method: Its Basis and Fundamentals. Oxford, UK: Elsevier, 2013.